Imaging and Radiation Research 2024, 7(1), 4546.
https://doi.org/10.24294/irr4546

Article

Differential diagnosis of hepatocellular carcinoma and cirrhotic nodules via radiomics models based on magnetic resonance images

Changdong Ma[1], Changsheng Ma[2,*], Shuang Yu[3,*]

[1] Department of Radiation Therapy, Qilu Hospital of Shandong University, Jinan 250012, China
[2] Department of Radiation Physics, Shandong First Medical University and Shandong Academy of Medical Sciences, Jinan 250012, China
[3] Department of Hematology, Qilu Hospital of Shandong University, Jinan 250012, China
*** Corresponding authors:** Changsheng Ma, machangsheng_2000@126.com; Shuang Yu, yushuang@sdu.edu.cn

CITATION

Ma C, Ma C, Yu S. Differential diagnosis of hepatocellular carcinoma and cirrhotic nodules via radiomics models based on magnetic resonance images. Imaging and Radiation Research. 2024; 7(1): 4546. https://doi.org/10.24294/irr4546

ARTICLE INFO

Received: 4 February 2024
Accepted: 9 April 2024
Available online: 30 April 2024

Abstract: Objective: To investigate the value of differential diagnosis of hepatocellular carcinoma (HCC) and cirrhotic nodules via radiomics models based on magnetic resonance images. **Background:** This study is to distinguish hepatocellular carcinoma and cirrhotic nodules using MR-radiomics features extracted from four different phases of MRI images, concluded T1WI, T2WI, T2 SPIR and delay phase of contrast MRI. **Methods:** In this study, the four kind of magnetic resonance images of 23 patients with hepatocellular carcinoma (HCC) were collected. Among them, 12 patients with liver cirrhosis were used to obtain cirrhotic nodules (CN). The dataset was used to extract MR-radiomics features from regions of interest (ROI). The statistical methods of MRradiomics features could distinguish HCC and CN. And the ability of radiomics features between HCC and CN was estimated by receiver operating characteristic curve (ROC). **Results:** A total of 424 radiomics features were extracted from four kind of magnetic resonance images. 86 features in delay phase of contrast MRI，86 features in spir phase of T2WI，86 features in T1WI and 88 features in T2WI showed statistical difference ($p < 0.05$). Among them, the area under the curves (AUC) of these features larger than 0.85 were 58 features in delay phase of contrast MRI, 54 features in spir phase of T2WI, 62 features in T1WI and 57 features in T2WI. **Conclusions:** Radiomics features extracted from MRI images have the potential to distinguish HCC and CN.

Keywords: radiomics features; hepatocellular carcinoma; MRI; cirrhotic

1. Introduction

The differential diagnosis of liver masses is still the current focus. As The primary liver cancer is one of the most common malignant tumors in the clinic, with more than 840,000 new cases per year and above 780,000 death cases per year, which incidence and mortality rate rank seventh and third in all cancers,respectively [1]. In more than 90% of the cases. The subtype of primary liver cancer is hepatocellular carcinoma (HCC) [2],which complicates liver cirrhosis caused by hepatitis C virus (HCV) and hepatitis B virus (HBV) infection [3]. The evolution of HCC is from cirrhotic nodule(CN) to dysplastic nodule(DN) and then to small hepatocellular carcinoma (SHCC), finally to progressed HCC [4]. SHCC also knowen as early hepatocellular carcinoma (eHCC) or subclinical hepatocellular carcinoma,without clearly imaging characterizations and clincial symptoms.The main reason of high mortality rate of HCC is detected so lately that treatment cannot work out effectively [5]. Thus, the sole approach to achieve long-term survival is to detect the tumor at an early stage.

Although biopsy is the gold standard for identifying focal hepatic lesions, it has limitations: a) Biopsy is an invasive examination, which have difficulity in acceptance of patients and repeatability of sample; b) The particularity of liver anatomy makes sampling difficult, appearing false-negative and false-positive results [5,6]; c) When the needle is withdrawn, it have risks to cause bleeding or implant transfer, which affects the subsequent treatment [6]. Fortunately, many researchers have discovered that the imaging features of SHCC and CN have great research value for differential diagnosis. Huang et al. [7] conclude that contrastenhanced ultrasound (CEUS) could be helpful in the differential diagnosis of hepatic malignant and benign lesions ,but dysplastic nodule may manifest with a similar enhancing pattern as that in welldifferentiated small HCC.Also,US images are easily affected by the operator's technical level and gastrointestinal gas. Chen et al. [8] concluded that 64-slice spiral CT can provide more sufficient imaging evidence for the clinical diagnosis of HCC and FNH and effectively identify benign and malignant tumors compared with conventional US examination, which also has high sensitivity in the diagnosis of tiny lesions.Furthmore, Ronot M and other researches [5] have shown that arterial phase hyperenhancement followed by washout on CT or MRI is highly specific.

However, whether CEUS, enhanced CT, it only distinguish CN from SHCC anatomically. With the continuous deepening of research, many researchers have now adviced that MRI functional imaging is useful for distinguishing diagnosis,which has great potential to research.For example, According to a study [9] of hepatocellular carcinoma based on US ,CTand MR images by some people, the sensitivity of MR images in the hepatobiliary stage is the highest. Moreover, the study on the quantitative evaluation of focal hepatic lesions by DWMRI used 4 b values to obtain different ADC images [10]. The results of the study suggest that ADC values can distinguish cavernous hemangioma and liver cysts. The ratio of the ADC value of leision/liver can distinguish HCC and hepatic metastasis, and can provide information to help diagnose focal hepatic lesions with a diameter less than 3 cm. However, these studies still cannot clearly distinguish SHCC from DN.Radiomics is an emerging technology that has developed in recent years. It uses software to extract the texture features of the region of interest(ROI) by delineating it in the image, and performs computer operations to obtain small image parameters that cannot be observed by the human eyes. This research will use the combination of radiomics and magnetic resonance technology to differentiate between DN and HCC.

2. Methods

2.1. Radiomics workflow

The raidomics flow of this study included: (1) images acquisition; (2) feature extraction; (3) data analysis **(Figure 1**).

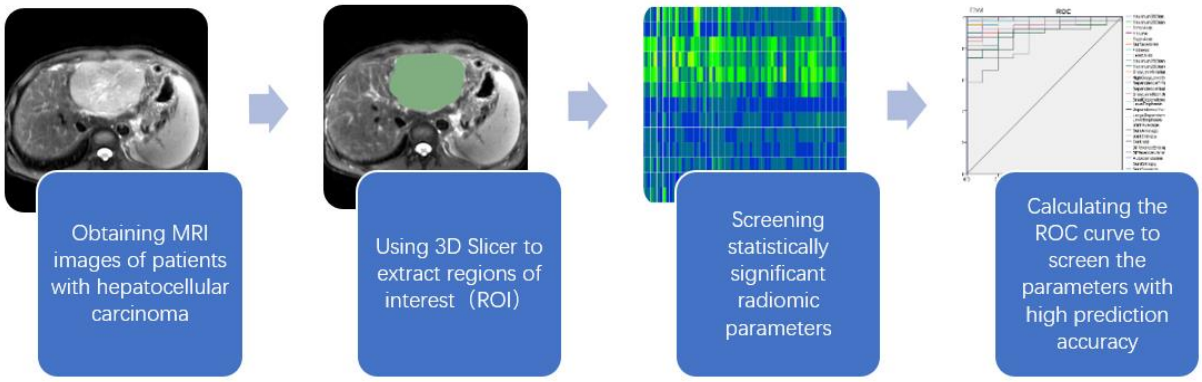

Figure 1. The workflow of the study.

2.2. Patients

The protocol for this study was approved by the Institutional Review Committee of the Shandong First Medical University Affiliated Cancer Hospital Ethics Committee. The ethics filing number is SDTHEC2020010008. Case entry criteria: (1) Complete clinical imaging data; (2) No surgery, radiotherapy, chemotherapy, or interventional treatment before imaging examination; (3) Pathologically confirmed hepatocellular carcinoma.Search for 23 patients with hepatocellular carcinoma in Shandong Cancer Hospital who met the enrollment criteria from April 2019 to January 2020, a total of 24 lesions, and they were recorded as 1 group, including 21 males and 2 females, aged 42–83 years old , An average of 56.08 years old. Among the above-mentioned patients, 12 had a history of liver cirrhosis and hepatitis B, and 12 had cirrhotic nodules, which were recorded as two groups, including 10 males and 2 females.

2.3. Patient images acquisition

Use GE HDe1.5TMR scanner.The scanning sequence and parameters are as follows: Axial breathing trigger FSETWI + FS,TR/TE2-3 breathing cycle/(80 ± 10) ms,layer thickness 6 mm, layer spacing 1.5 mm, field of view (FOV) 40 cm × 36 cm, matrix 320 × 224, number of excitations 2; SE. EPIDWI, TR 5000 ms, TE 75.40 ms, layer thickness 6 mm, layer spacing 1.5 mm, FOV 40 cm × 40 cm, matrix 128 × 128, number of excitations 8; FSPGR TWI inverse phase imaging, TR 120–250 ms, TE 2.25–4.5 ms, layer thickness 6 mm, layer spacing 1.5 mm, FOV 40cm×36 cm, matrix 256 × 170, excitation times 1; Liver Volume Rapid Acquisition (IAVA) three-dimensional dynamic enhancement scan, TR 5.14 ms, TE 2.30 ms,The layer thickness is 5 mm, the layer spacing is 2.50 mm, the FOV is 40 cm × 36 cm, and the matrix is 288 × 192. Using a double-barreled high-pressure syringe, inject Ou Naiying 0.1 mol/kg body weight through the cubital vein at a flow rate of 3 ml/s, and scan the arterial phase, portal vein phase, and equilibrium phase at 18–22 s, 60 s, and 180 s after the contrast agent injection. The size of the liver is about 15–18s to complete a single-phase whole liver scan.

2.4. Region of interests (ROI) segmentation

The images are divided into four categories: T1WI, T2WI, T2 SPIR, and enhanced scan delay period. Two imaging physicians with more than 5 years of work

experience observe all the images separately, and those who have different results discuss and reach an agreement together. Use the imaging omics analysis software 3D slicer 4.8 to delineate the area of interest and obtain 106 children with seven parent features The characteristic data table, the area of interest (ROI)

Of the lesion includes the largest extent of the lesion entity as much as possible, and avoids the blood vessel, hemorrhage, necrosis, and cystic area.Divide the data into four categories:T1WI, T2WI, T2 SPIR, and enhanced scan delay period, and then divide each category into seven groups: Shape, Gldm, Glcm, Firstorder, Glrlm, Glszm, and Ngtdm, and analyze them separately.

3. Statistical analysis

Enter the values of all parameters into html to obtain a heat map representing these data.(**Figure 2**) The statistical analysis software SPSS 22.0 was used to process and analyze the data. Mann-Whitney U test was selected for the imaging omics characteristic parameter data obtained from the MR images of each phase of the cancer and sclerosing nodules to screen

for statistically significant difference parameters between the two lesions. Thus obtained radiological characteristics that can distinguish hepatocellular carcinoma from sclerosing nodules. Then use the ROC curve drawing function in spss to determine the diagnostic performance of the above-mentioned characteristic parameters. The characteristic parameters whose area under the curve is less than 0.85 are eliminated. Thus, imaging characteristics parameters that can efficiently distinguish hepatocellular carcinoma from sclerosing nodules can be obtained.

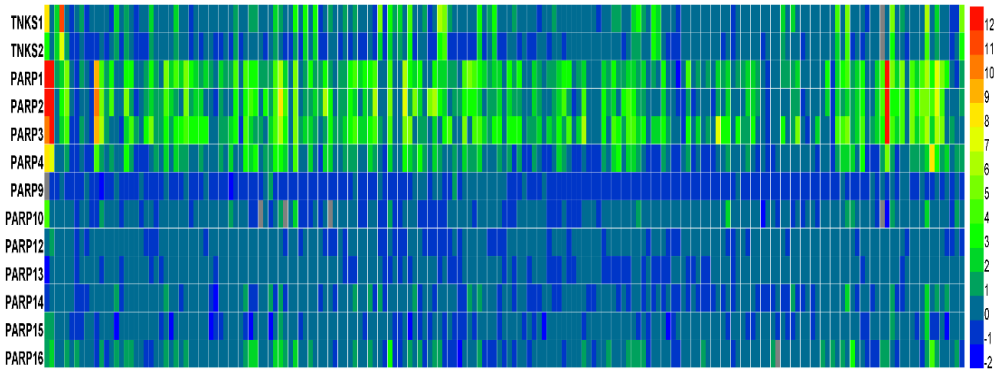

Figure 2. Distribution of all parameters.

3.1. Patient characteristics

In this study, a total of 23 hepatocellularcarcinoma patients were included, including 21 men and 2 women (maximum age 83 years, minimum age 42 years, median age 53 years). Then there are 12 patients with a history of liver cirrhosis among these 23 patients, of which 10 are males and 2 are females (maximum age 66 years, minimum age 42 years, median age 56 years). See **Table 1**.

Table 1. Clinical information of enrolled patients.

Number	Age	Sex	Size (cm)	T1WI	T2WI	T2 SPIR	DELAY	Cirrhosis	Hepatitis
1	62	M	3.0 × 3.0	--	--	√	√	--	--
2	64	M	5.8 × 6.6	--	√	√	√	--	--
3	42	M	2.0 × 1.5	--	√	√	--	positive	HBV
4	63	M	4.6 × 7.0	--	√	√	√	--	HBV
5	49	M	10.2 × 7.6	√	√	√	--	positive	HBV
6	83	M	0.9 × 1.6	√	√	√	--	--	--
7	44	M	4.8 × 6.2	--	√	√	√	positive	HBV
8	56	M	3.3 × 2.5	--	√	√	√	--	HBV
9	58	M	9.3 × 9.0	--	√	√	√	positive	HBV
10	58	M	1.4 × 0.9	--	√	√	--	positive	HBV
11	53	M	2.6 × 2.4	√	√	√	--	positive	HBV
12	62	M	6.9 × 5.0	√	√	√	--	--	HBV
13	49	M	3.2 × 2.9	--	√	√	√	Positive	HBV
14	66	F	2.8 × 2.8	--	√	√	√	Positive	HBV
15	58	F	4.4 × 3.5	√	√	√	--	Positive	HBV
16	48	M	8.0 × 5.1	√	√	√	--	Positive	HBV
17	50	M	2.7 × .3	--	√	√	√	Positive	HBV
18	46	M	14.1 × 9.8	--	√	√	√	-	HBV
19	50	M	8.2 × 8.4	--	√	√	√	Positive	Positive
20	42	M	9.9 × 7.2	√	√	√	--	Positive	positive
21	67	M	7.2 × 6.6	√	√	√	--	-	HBV
22	60	M	10.9 ×8.5	--	√	√	√	Positive	HBV
23	60	M	11.0 × 10.5	√	√	√	--	Positive	HBV

4. Feature results

In this study, a total of 106 imaging radi-omics features of 24 hepatocellular carcinomalesions and 12 sclerosing nod-ules lesions were extracted. According to the imaging omics, these 106 features can be divided into 7 catgories. Be more detailed,shape 13 features, gldm 14 features,glcm 24 fetures, firstorder 18 features,glrlm 15 features,glszm 16 fea-tures, ngtdm 5 features.

4.1. Statistical results

All data have been tested by the Mann-Whitney U test, and the *p*-values obtained are shown in **Table 2**. As shown in **Table 2**, among all four imaging methods, there are 70 types of statistically significant differences in imaging features between hepatocellular carcinoma and cirrhotic nodules. They were 86 features in T1WI and 88 features in T2WI, 86 features in delay phase of con-trast MRI and 86 features in spir phase of T2W.

Table 2. Feature parameters and differentiating between cirrhotic nodules and hepatocellular carcinoma.

Category	Feature	T1wI	P value	DELAY	TIWI	T2WI	ROCSPIR	DELAY
	Maximum3DDiameter	0.001	T2WI	0.044	1	1	SPIR	0.792
	Maximum2DDiameterSlice	0.001	0	0.011	1	1	0.958	0.857
	MinorAxis	0.001	0	0	1	1	0.955	1
	Volume	0.001	0	0	1	1	1	1
shape	MajorAxis	0.001	0	0.104	1	1	1	0.74
	SurfaceArea	0.001	0	0	1	1	0.955	1
	Flatness	0.003	0	0	0.96	0.992	1	1
	LeastAxis	0.001	0	0	1	0.996	1	1
	Maximum2DDiameterColumn	0.001	0	0	1	1	1	1
	Maximum2DDiameterRow	0.001	0	0	1	1	1	1
	GrayLevelVariance	0.003	0	0.011	0.96	0.995	1	0.857
gldm	HighGrayLevelEmphasis	0.001	0	0.004	1	1	0.966	0.896
	DependenceEntropy	0.001	0	0	1	1	0.992	1
	DependenceNonUniformity	0.001	0	0	1	1	1	1
	GrayLevelNonUniformity	0.001	0	0	1	0.963	1	1
	SmallDependenceHighGrayLevelEmphasis	0.594	0.203	0.006	0.6	0.889	0.992	0.883
	LargeDependenceEmphasis	0.008	0	0.002	0.92	0.829	0.777	0.922
	DependenceVariance	0.008	0.001	0	0.92	0.945	0.818	0.974
	LargeDependenceHighGrayLevelEmphasis	0.001	0	0.002	1	1	0.958	0.922
	JointAverage	0.001	0	0.002	1	1	1	0.922
glcm	SumAverage	0.001	0	0.002	1	1	0.996	0.922
	JointEntropy	0.003	0	0	0.96	0.997	0.996	1
	Idmn	0.594	0	0.011	0.4	0.655	0.977	0.857
	Contrast	0.04	0.072	0	0.84	0.934	0.939	0.961
	DifferenceEntropy	0.005	0	0	0.94	0.966	0.886	1
	DifferenceVariance	0.005	0	0	0.94	0.966	0.958	1
	Idn	0.594	0	0.011	0.4	0.582	0.951	0.857
	Correlation	0.594	0.35	0	0.4	0.655	0.773	1
	Autocorrelation	0.001	0.062	0.004	1	1	0.97	0.896
	SumEntropy	0.001	0	0	0.98	1	0.996	1
firstorder	SumSquares	0.003	0	0.006	0.96	0.982	1	0.883
	ClusterProminence	0.001	0	0.008	1	1	0.947	0.87
	Imc2	0.001	0	0.375	0.98	0.645	0.977	0.636
	DifferenceAverage	0.055	0.076	0.002	0.82	0.889	0.61	0.922
	ClusterTendency	0.001	0	0.006	1	0.997	0.833	0.883
	InterquartileRange	0.001	0	0.011	1	0.963	0.966	0.857
	Energy	0.001	0	0	1	1	0.909	1
	RobustMeanAbsoluteDeviation	0.001	0	0.011	1	0.966	0.992	0.857
	MeanAbsoluteDeviation	0.001	0	0.011	1	0.984	0.928	0.857
	TotalEnergy	0.001	0	0	1	1	0.962	1
	Maximum	0.001	0	0	0.88	0.958	0.992	1

Table 2. (*Continued*).

Category	Feature	T1wI	P value	DELAY	TIWI	T2WI	ROCSPIR	DELAY
	90Percentile	0.055	0	0.003	0.44	0.842	0.788	0.909
	Entropy	0.001	0.001	0	0.96	1	0.648	1
	Range	0.003	0	0.002	1	1	0.985	0.922
glszm	Variance	0.001	0	0.011	1	0.995	0.996	0.857
	Kurtosis	0.001	0	0.104	0.94	0.897	0.966	0.74
	GrayLevelVariance	0.001	0	0.011	1	0.995	0.837	0.857
	GrayLevelNonUniformityNormalized RunVariance	0.001	0	0	1	0	0.966	0
	LongRunEmphasis	0.001	SPIR	0.211	1	0.653	0.011	0.688
ngtdm	ShortRunHighGrayLevelEmphasis	0.008	0	1	0.92	1	0.659	0.494
	RunLengthNonUniformity	0.001	0	0.004	0.98	0.503	0.534	0.896
	LongRunHighGrayLevelEmphasis	0.001	0	0	1	1	0.981	1
	RunEntropy	0.001	0	0.008	1	1	1	0.87
	HighGrayLevelRunEmphasis	0.001	0	0	1	1	1	1
	GrayLevelVariance	0.001	0	0.006	1	1	1	0.883
	ZoneVariance	0.001	0	0.011	1	0.997	0.992	0.857
	SizeZoneNonUniformity	0.001	0	0	1	0.971	1	1
	GrayLevelNonUniformity	0.001	0	0	1	0.992	0.966	1
	LargeAreaEmphasis	0.001	0	0	1	1	0.962	1
	SmallAreaHighGrayLevelEmphasis	0.005	0	0	0.94	0.916	1	0.974
	LargeAreaLowGrayLevelEmphasis	0.001	0	0.002	1	0.989	0.939	0.922
	LargeAreaHighGrayLevelEmphasis	0.008	0	0.479	0.92	0.663	0.939	0.61
	HighGrayLevelZoneEmphasis	0.001	0	0	1	1	0.583	0.961
	SmallAreaEmphasis	0.001	0	0.008	1	1	1	0.87
	ZoneEntropy	0.001	0.002	0.659	1	0.561	0.989	0.429
	Complexity	0.001	0.002	0	1	1	0.485	1
	Busyness	0.001	0	0	0.98	0.989	1	1
		0.003	0	0.246	0.96	0.947	0.989	0.675
			0				0.807	
			0					
			0					
			0					
			0					
			0					
			0					
			0.009					
			0					
			0					
			0					
			0					
			0					
			0.316					

Table 2. (*Continued*).

Category	Feature	T1wI	P value	DELAY	TIWI	T2WI	ROCSPIR	DELAY
			0.001					
			0					
			0					
			0					
			0					
			0					
			0					
			0.006					
			0.174					
			0					
			0					
			0					
			0.001					
			0					
			0					
			0.142					
			0.766					
			0					
			0					
			0					
			0					
			0					
			0					
			0					
			0					
			0					
			0					
			0					
			0					
			0.451					
			0					
			0					
			0.903					
			0					
			0					
			0.003					

A ROC curve of 105 features was performed to evaluate the ability of the features to distinguish hepatocellular carci noma from sclerosing nodules. This curve (AUC < 0.85) was abandoned in this study due to its limited discriminative ability. In the end, this study obtained a total of 68 characteristic ROC curves (**Figures 3**–**6**).

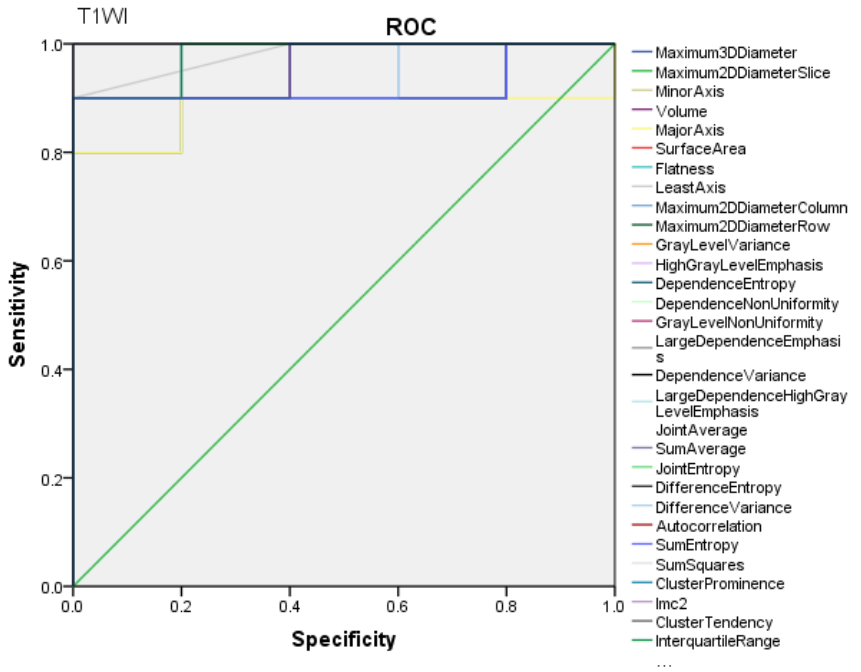

Figure 3. The ROC curves of T1WI.

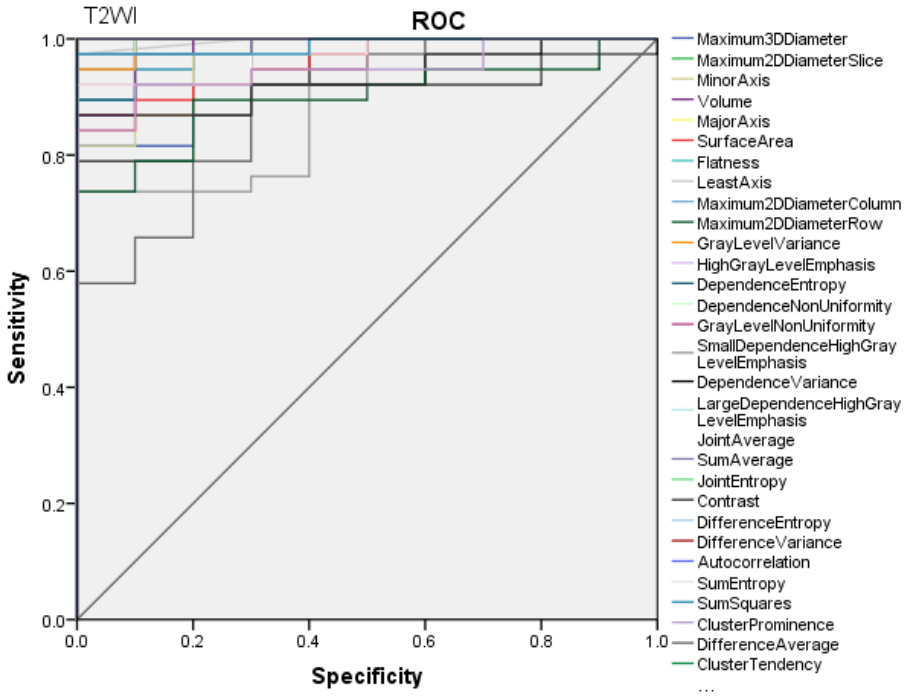

Figure 4. The ROC curves of T2WI.

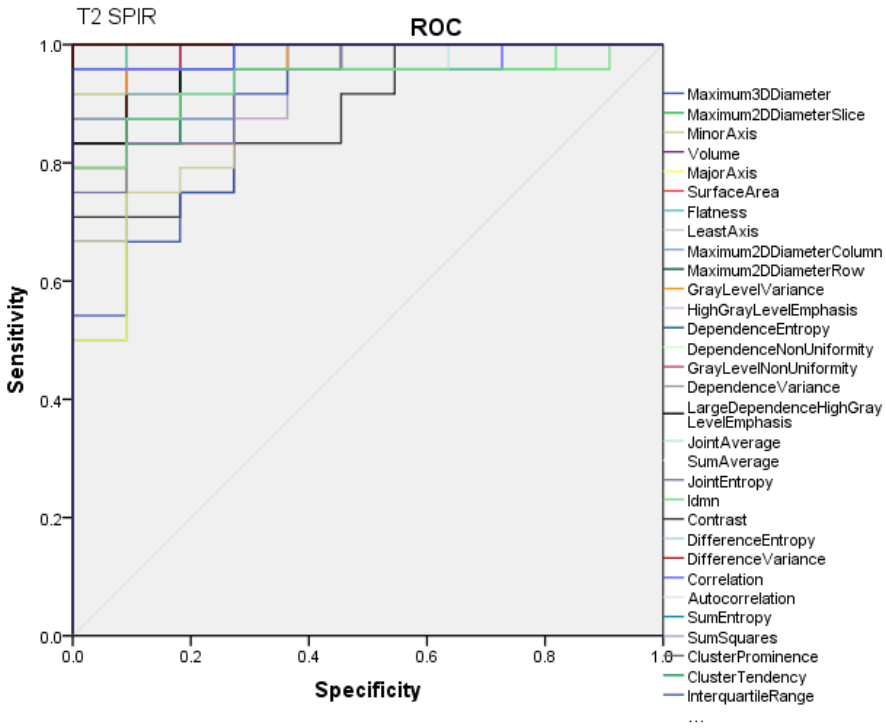

Figure 5. The ROC curves of SPIR.

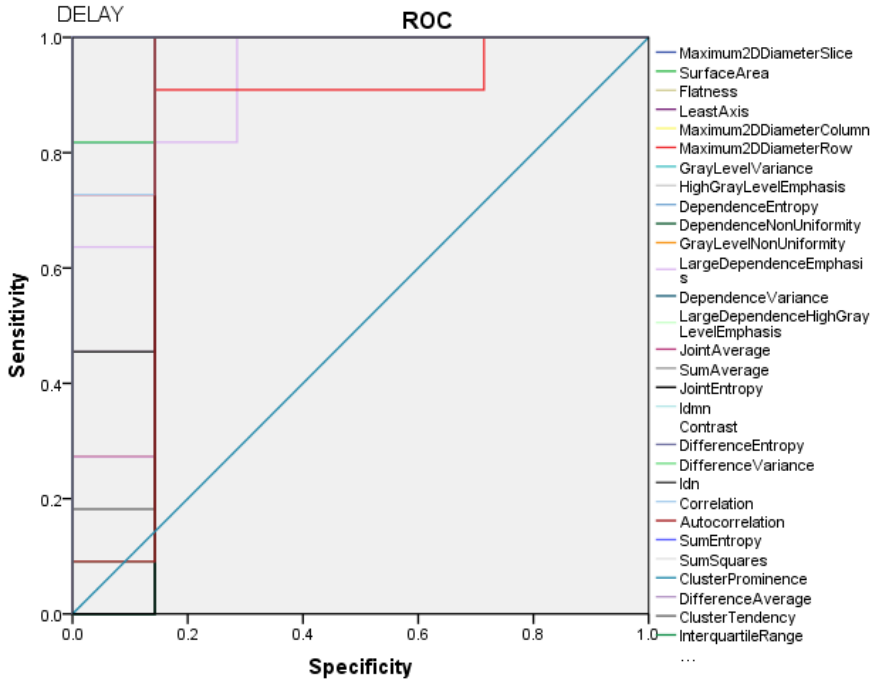

Figure 6. The ROC curves of DELAY.

5. Discussion

The results of this study show that there is a statistical difference between thera-diographic features extracted from hepa-tocellular carcinoma lesions and thera-diographic features extracted from cir-rhotic nodules. This maybe related to their different pathological tissue morphology. Carcinogenesis is a process in which non-

malignant liver cells gradually transform into liver cancer, which is a complex and multi-step process. For clinical practicability and research, this process is divided into several independ-ent steps: Cirrhotic nodules, dyplastic nodules, early liver cancer, and pro-gressed liver cancer [11]. This study selects the stage of cirrhotic nodules. Cirrhosis nodules,also called regenerative nodules related to liver cirrhosis,are countless clear circular areas of hard-enedparenchyma with scar tissue around them, with a diameter of 1–15 mm [11]. Cirrhotic nodules are generally considered benign because of its lacking histological features and normal phenotype [12]. But from a molecular perspective, many cirrhotic nodules are the clonal expansion of abnormal genomic cells, causing the macrophages in the cirrhotic nodules to develop abnormal proliferation characteristics [13]. So it will cause hyperplasia and nodules. A large number of previous studies have shown that the molecular changes of liver cells caused by abnormalities such as cell sig-nal transduction caused by chronic in-flammation begin in the early stage of tumor formation [14–16]. That is, several years or even decades before the onsetof liver cirrhosis, and with the development of fibrosis and cirrhosis Parallel development [17,18]. Studies have shown that the earliest molecular change in liver cancer is morphological silence, suggesting that chronically ill liver may contain cells with abnormal molecular but normal phenotypes, which will eventually develop into liver cancer [13,18,19]. Pathologically, early HCC is composed of small, well-differentiated neoplastic cells arranged in irregular but thintra-beculae or pseudogland [20], microscopically similar to highly hyperplastic nodules [21]. The tissues of advanced liver cancer lesions have the characteristics of mosaic structure, that is, there are multi-ple tumor nodules inside, and these nodules are separated by fibers, and there are areas of hemorrhage, necrosis, and occasional steatosis [22]. The subtle differences in histology between hepatocellu-lar carcinoma and cirrhotic nodules can be distinguished on MR.

The radiomics technology that has emerged in recent years refers to the high-throughput extraction of a large number of image features describing tumor characteristics, and the application of a large number of automated data retention methods to convert the image data of the region of interest into high-resolution imaging data. Feature space data sent [23,24]. Data analysis is a digital quantitative high-throughput analysis of a large amount of image data to obtain high-fidelity target information to comprehensively evaluate various phenotypes of tumors, including tissue morphology, cell molecular, genetic inher-itance and other levels. The core theo-retical basis is the radiomic model,which contains the biological or medical data information of the lesion, which can provide valuable information for the diagnosis, prognosis and prediction of the disease [25,26]. There is genetic heterogeneity among tumors of different patients, different tumor tissues of the same patient, or within the same tumor, and their genetic status will also vary from time to time. Based on the above advantages,some researchers have combined radiomics with medical images and applied them to tumor prediction, identification and prognosis. Imageomics has shown excellent performance in the diagnosis of lung cancer [27], stomach cacer [28], prostate cancer [29], and breast cancer [27]. Tsai et al. [30] reported that Texture features can be used to distinguish nasopharyngeal carcinoma from normal nasopharyngeal tissue, and the statistical difference in texture features between nasopharyngeal carcinoma and normal nasopharyngeal tissue maybe related to the loss

of stripe structure in normal nasopharyngeal tissue. and this finding had been confirmed on MRI images. Thawani et al. proposed that radiomics has played an important role in the diagnosis of lung cancer in recent years and will further provide more important information for monitoring and prognosis, and realize individualized treatment [31,32].

6. Conclusions

The results of this study show that MR is of great significance for the diagnosis of liver cancer, and imaging omics is of great value in the differentiation between benign and malignant lesions.However, the research method in this ar-ticle has limitations: (1) This article uses a single-center study with a small number of samples; (2) Lack of differentiation from patients without liver cancer; (3) Not combined with patient pathologi-cal smears; (4) Only one kind of imaging is used Methods, failed to compare the sensitivity and specificity of different imaging techniques to lesions. Our later research will try multi-center research to obtain a large number of samples based on more imaging methods to improve the accuracy of the results.

Author contributions: Conception and design, CM (Changdong Ma); administrative support, SY; provision of study materials or patients, CM (Changsheng Ma); collection, CM (Changsheng Ma); assembly of data, CM (Changdong Ma); data analysis, CM (Changsheng Ma); interpretation, CM (Changdong Ma); manuscript writing, CM (Changdong Ma); final approval of the manuscript, CM(Changdong Ma), CM (Changsheng Ma) and SY. All authors have read and agreed to the published version of the manuscript.

Ethical approval: The study was conducted in accordance with the Declaration of Helsinki. The protocol for this study was approved by the Institutional Review Committee of the Shandong First Medical University Affiliated Cancer Hospital. The ethics filing number is SDTHEC2020010008. As this is a retrospective study and sensitive information of all patients was hidden during the study process, so the need for informed consent was waived by the Institutional Review Committee of the Shandong First Medical University Affiliated Cancer Hospita (SDTHEC2020010008).

Availability of data and materials: The datasets used and analyzed during the current study available from the corresponding author on reasonable request (machangsheng_2000@126.com).

Funding: This study was supported by the National Nature Science Foundation of China (81974467), the Natural Science Foundation of Shandong Province (ZR2023MH166).Shandong Medical Association Clinical Research Fund-Qilu Special Project (YXH2022ZX02197), Shandong Traditional Chinese Medicine Technology Project (M-2022225).

Conflict of interest: The authors declare no conflict of interest.

Abbreviations

CT	Computed Tomography
MRI	Magnetic Resonance Imaging
DWI	Diffusion Weighted Imaging
T2WI	T2-Weighted Imaging
ROI	Region of Interest;
VOI	Volume of Interest;
ROC	Receiver Operating Characteristic;
AUC	Area Under the Curve
GLRLM	Gray Level Run Length Matrix;
GLCM	Gray Level Co-occurrence Matrix
GLSZM	Gray Level Size Zone Matrix
NGTDM	Neighborhood Gray-Tone Difference Matrix
GLD	Gray Level Dependence Matrix
CEUS	Contrast-enhanced Ultrasound
TR	Repetition Time
TE	Echo Time

Reference

1. Bray F, Ferlay J, Soerjomataram I, et al. Global cancer statistics 2018: GLOBOCAN estimates of incidence and mortality worldwide for 36 cancers in 185 countries. CA Cancer J Clin. 2018; 68(6): 394–424. doi:10.3322/caac.21492
2. McGlynn KA, London WT. Epidemiol-ogy and natural history of hepatocellu-lar car cinoma. Best Pract Res Clin Gas-troenterol. 2005;19(1): 3–23.
3. Theise ND, Curado MP, Franceschi S, et al. Hepatocellular carcinoma. In: Bosman FT, Carneiro F, Hruban RH, Theise ND. (editors). WHO Cassification of Tumours of the Di gestive System. IARC Publishing; 2010. pp. 205–216.
4. Choi JY, Lee JM, Sirlin CB. CT and MR imaging diagnosis and staging of hepatocellular carcinoma: part I. Devel-opment, growth, and spread: Key path-ologic and imaging aspects. Radiology. 2014; 272(3): 635–654.
5. Ronot M, Purcell Y, Vilgrain V. Hepato-cellular Carcinoma: Current Imaging Modalities for Diagnosis and Prognosis. Dig Dis Sci. 2019; 64(4): 934–950. doi:10.1007/s10620-019-05547-0
6. Forner A, Vilana R, Ayuso C, et al. Diag nosis of hepatic nodules 20 mm or smaller in cirrhosis: Prospective valida-tion of the noninvasive diagnostic cri-teria for hepato cellular carcinoma. Hepatology 2008; 47(1): 97–104.
7. Huang JY, Li JW, Lu Q, et al. Diagnostic Accuracy of CEUS LI-RADS for the Characterization of Liver Nodules 20 mm or Smaller in Patients at Risk for Hepatocellular Carcinoma. Radiology. 2020; 294(2): 329–339.
8. Chen X, Yang Z, Deng J. Use of 64-Slice Spiral CT Examinations for Hepatocel-lular Carcinoma (DR LU). J BUON. 2019; 24(4): 1435–1440
9. Di Martino M, De Filippis G, De Santis A, et al. Hepatocellular carcinoma in cir-rhotic patients: prospective comparison of US, CT and MR imaging. Eur Radiol. 2013; 23(4): 887–896. doi:10.1007/s00330-012-2691-z
10. Sun XJ, Quan XY, Huang FH, Xu YK. Quantitative evaluation of diffusion-weighted magnetic resonance imaging of focal hepatic lesions. World J Gastro-enterol. 2005; 11(41): 6535–6537. doi:10.3748/wjg.v11.i41.6535
11. International Working Party. Terminol-ogy of nodular hepatocellular lesions. Hepatol ogy. 1995; 22(3): 983–993.
12. Park YN, Kim MJ. Hepatocarcinogenesis: imaging-pathologic correlation. Ab-dom Im aging 2011; 36(3): 232–243.
13. Aihara T, Noguchi S, Sasaki Y, Nakano H, Imaoka S. Clonal analysis of regen-erative nodules in hepatitis C virus-in-duced liver cirrhosis. Gastroenterology. 1994; 107(6): 1805– 1811.
14. Trevisani F, Cantarini MC, Wands JR, Bernardi M. Recent advances in the nat ural history of hepatocellular carcinoma. Carcinogenesis. 2008; 29(7): 1299–1305.
15. Brody RI, Theise ND. An inflammatory proposal for hepatocarcinogenesis. Hepa tology 2012; 56(1): 382–384.

16. Thorgeirsson SS, Grisham JW. Molecu-lar pathogenesis of human hepatocel-lular car cinoma. Nat Genet, 2002; 31(4): 339–346.
17. Theise ND. Macroregenerative (dys-plastic) nodules and hepatocarcino-genesis: theo retical and clinical consid-erations. Semin Liver Dis .1995;1 5(4): 360–371.
18. Aravalli RN, Cressman EN, Steer CJ. Cel lular and molecular mechanisms of hepato cellular carcinoma: An update. Arch Toxicol. 2013; 87(2): 227–247.
19. Sun M, Eshleman JR, Ferrell LD, et al. An early lesion in hepatic carcinogenesis: loss of heterozygosity in human cir-rhotic livers and dysplastic nodules at the 1p36-p34 region. Hepatology .2001; 33(6): 1415–1424.
20. Park YN. Update on precursor and early lesions of hepatocellular carcinomas. Arch Pathol Lab Med. 2011; 135(6): 704–715.
21. Roskams T, Kojiro M. Pathology of early hepatocellular carcinoma: conventional and molecular diagnosis. Semin Liver Dis 2010; 30(1): 17–25.
22. Stevens WR, Gulino SP, Batts KP, et al. Mosaic pattern of hepatocellular carcinoma: histologic basis for a characteristic CT appearance. J Com put Assist Tomogr. 1996; 20(3): 337–342.
23. Lambin P, Rios-Velazquezet E, Leijenaaral R, et al. Radiomics: extracting more information from medical images using advanced feature analysis. European Journal of Cancer. 2012; 48: 441–446.
24. Kumar V, Gu Y, Basu S, et al. Radiomics: the process and the challenges. Magn. Reson. Im-aging. 2012; 30, 1234–1248.
25. Haase AT, Henry K, Zupancic M, et al. Quantitative image analysis of HIV-1 infection in lymphoid tissue. Science. 1996; 274, 985–989.
26. Schoolman H, Bernstein L. Com-puter use in diagnosis, prognosis, and therapy. Science. 1978; 200: 926–931.
27. Avanzo M, Stancanello J, Pirrone G, Sartor G. Radiomics and deep learning in lung cancer. Strahlenther Onkol. 2020; 196(10): 879–887. doi:10.1007/s00066-020-01625-9
28. Jiang Y, Chen C, Xie J, et al. Radiomics signature of computed tomography imaging for prediction of survival and chemotherapeutic benefits in gastric cancer. EBioMedicine. 2018; 36: 171–182. doi:10.1016/j.ebiom.2018.09.007
29. Smith CP, Czarniecki M, Mehralivand S, et al. Radiomics and radiogenomics of prostate cancer. Abdom Radiol (NY). 2019; 44(6): 2021–2029. doi:10.1007/s00261-018-1660-7
30. Tsai A, Buch K, Fujita A, et al. Using CT texture analysis to differentiate between naso-pharyngeal carcinoma and age-matched adenoid controls. Eur J Radiol. 2018; 108: 208–14.
31. Thawani R, McLane M, Beig N, et al. Radiomics and radiogenomics in lung cancer: A review for the clinician. Lung Cancer. 2018; 115: 34–41. doi:10.1016/j.lungcan.2017.10.015
32. Wei K, Su H, Zhou G,et al. Potential application of radiomics for differentiating solitary pul-monary nodules,OMICS J Radiol. 2016; 5(2): 1000218